Modeling Grouted Sand Under Torsional Loading

CUMARASWAMY VIPULANANDAN AND RAYMOND J. KRIZEK

The mechanical behavior of grouted sand is controlled by some combination of the properties of grout, sand, and their interaction. In this study, chemically grouted sand is considered a two-phase particulate composite, and the mechanical properties under pure torsional loading are examined at both the particulate and composite levels. Both the adhesive and cohesive properties of grout are believed to influence the behavior of grouted sand, and an experimental program was conducted to quantify the particular relationship for each. These data, together with the porosity of the sand, are employed to formulate strength, shear modulus, and failure strain models for predicting the behavior of grouted sand from a knowledge of the properties of the constituents. The most critical mode of failure for grout and grouted sand is tension, but comparisons are also made between the shear and compressive properties.

The extensive use of chemical grouts in recent years to solve a multitude of geotechnical engineering problems has dictated the need for a better understanding of the behavior of the grouted sand under different loading conditions. Most studies have been limited to the behavior of grouted sand in compression with very little emphasis on understanding the mechanisms responsible. As one step toward better understanding the complicated interaction between the sand and the grout, a detailed experimental study was undertaken of the adhesive and cohesive properties of grout and the mechanical properties of grouted sand under torsional loading. The mechanical properties of interest are the strength, failure strain, modulus, and critical mode of failure. Adhesive tests described in an earlier study are used to evaluate the adhesive properties, and torsional tests are used in this study to investigate the mechanical properties of grout and grouted sand.

OBJECTIVES

The objectives of this study are *(a)* to evaluate the respective contributions of sand and grout, as well as their interaction on the overall behavior of grouted sand under torsional loading, *(b)* to use the properties of the constituents in the formulation of models for predicting the shear response of grouted sand, and *(c)* to study the variation in the mechanical properties of grout and grouted sand with curing time.

MATERIAL SELECTION

Because the purpose of this investigation was to improve understanding of the mechanisms influencing the behavior of grouted sand under torsional loading, the materials were limited to one chemical grout and one sand. The grout mix consisted of hydrated sodium silicate ($Na_2SiO_3 \cdot nH_2O$), water (H_2O), formamide ($HCONH_2$) and ethyl acetate ($CH_3COOC_2H_5$) proportioned according to volume in the ratio of 10:8:1:1; the gel time of this grout mix was about 15 min at room temperature (20°C ± 2°C). The sand was Ottawa 20-30, which is composed of almost pure quartz and has a uniformity coefficient of 1.08.

METHOD OF TESTING

In the absence of standard tests to evaluate the shear properties of either grout or grouted sand, testing techniques were developed to obtain the required measurements. Two types of tests were employed: one to measure the shear properties of the grout and grouted sand and the other to measure the adhesive strength (bond strength).

Hollow Cylinder Torsional Test

The torsional test used herein subjects a specimen to all three forms of stress simultaneously, and the manner of failure will be governed by the critical strength. Materials that are weaker in shear than in compression or tension will fail in shear, whereas materials that are weaker in tension than in compression or shear will fail in tension. When a specimen is loaded in pure torsion, the material will be subjected to equal magnitudes of shear, compression, and tensile stresses, and the specimen will fail in its critical mode, as shown in Figure 1. During pure torsional loading, the directions of the principal stresses are unchanged. A torsional test allows measurement of the applied torque and angular deflection, and hence constitutive relationships can be developed. In this experimental program, a torsional test on a hollow cylindrical specimen was employed, as shown in Figure 2.

The stress distribution within a hollow cylindrical specimen

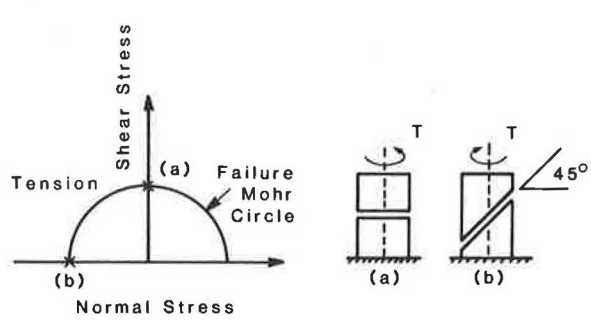

FIGURE 1 Critical modes of failure under pure torsional loading *(a)* shear failure and *(b)* tensile failure.

C. Vipulanandan, Cullen College of Engineering, University of Houston, University Park, Houston, Tex. 77004. R. J. Krizek, Department of Civil Engineering, Northwestern University, Evanston, Ill. 60201.

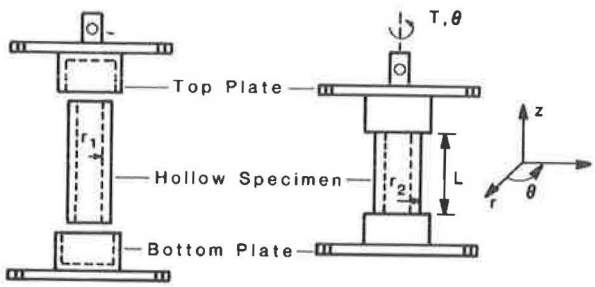

FIGURE 2 Torsional test configuration.

will depend on its material properties, specimen geometry (inner and outer radii and height), and end restraints *(1, 2)*. Because of the low strength and brittleness of the grout and grouted sand limitations associated with specimen preparation and handling, it was decided to adopt a ratio of inner to outer radius of 0.5. Figure 3 compares the selected dimensions with geometries used by other researchers *(2)*. The length of the specimen should be as long as possible so that a large region will exist that will not be affected by the end restraints. In general, however, the stability of a specimen and experimental difficulties will govern its height. The effective height, L, of the specimens used in these tests varied between $3.5r_2$ to $4r_2$.

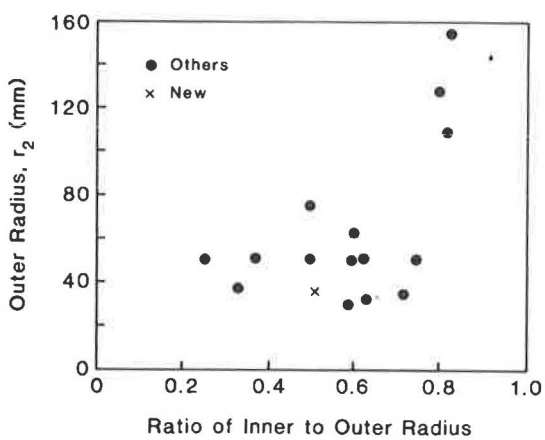

FIGURE 3 Geometries of specimen used in earlier hollow cylinder apparatuses.

Simple averaging will be used in reducing the data. Hence, the average shear strain is given by

$$\gamma_{\theta z} = [(r_1 + r_2)/2]\ \theta/L \qquad (1)$$

where θ is the angle of twist and r_1, r_2, and L are the specimen dimensions, as shown in Figure 2. If T is the twisting moment, equilibrium demands that

$$T = \int_A \tau_{z\theta}(r)\, dA\, r = 2_\pi \int_{r_1}^{r_2} \tau_{z\theta}(r)\, r^2 dr \qquad (2)$$

Assuming the stress to be uniform, which is generally justified for a thin-wall cylindrical specimen, will result in

$$\tau_{z\theta} = 3T/[2_\pi (r_2^3 - r_1^3)] \qquad (3)$$

This uniform shear stress and average shear strain will be used in all calculations.

Adhesion Test

The physical and chemical interaction of two or more materials at their interface is known as adhesion or bonding. In this case the sand surface will be modeled by a quartz rock with a chemical composition similar to that of sand, and simple tests proposed by Krizek and Vipulanandan *(3)* will be used to determine the adhesive strength. Both tensile and shear failures are possible under torsional loading, and the adhesive tensile and shear strengths will be of concern in this study.

The tensile test consisted of sandwiching a layer of grout between flat surfaces of quartz rock, as shown in Figure 4*a*. For this type of test, equilibrium considerations dictate that the average adhesive tensile (AT) stress at failure, σ_{tf}^{AT}, across the interface in the axial direction must be P/A where P is the maximum applied load and A is the cross-sectional area. The adhesive shear strength was evaluated by use of a torsional test, which consisted of subjecting an inner rock core to torsion while holding fixed an outer surface, with grout filling the intermediate annulus, as shown in Figure 4*b*. Because the radial displacement is zero within the grout and there is no warping of the cross section, the grout area will remain constant and this loading will induce a relatively pure shear condition within the grout. When this configuration is subjected to a torque, T, equilibrium at the inner surface demands that

$$T = \int_0^L (2\pi r_1\, dz)\, \tau_{r\theta}(z)\, r_1 = 2\pi r_1^2 \int_0^L \tau_{r\theta}(z)\, dz \qquad (4)$$

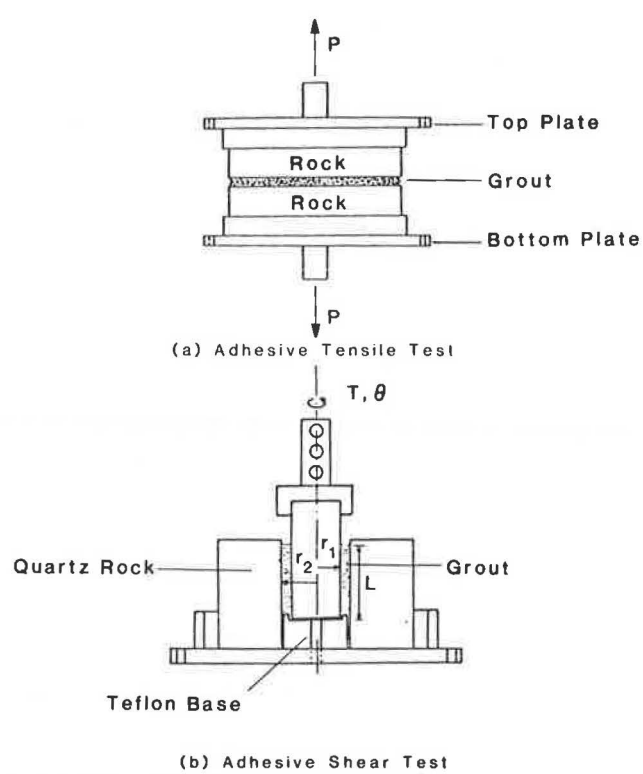

FIGURE 4 Adhesive test configurations.

Because the rock is much stiffer than the grout with a no-slip condition assumed at the interface, all points on the interface are subjected to the same angular displacement, which implies a uniform stress distribution as follows:

$$\tau_{r\theta} = T/2\pi r_1^2 L \quad (5)$$

As the gap between the rock surfaces is small (about 1.8 mm), the shear stress at the inner and outer interfaces, as well as within the grout, will be almost equal.

PROPERTIES OF GROUT

Pure grout (PG) specimens were tested in unconfined torsion after different periods of curing in a humid temperature-controlled room. Hollow specimens were made by inserting a nylon rod concentrically into a 6-in. long, 1.5-in. diameter PVC tube that was closed with rubber stoppers at the bottom and sealed at the top with waxed paper. These rods were subsequently removed with a small twist before the specimens were glued to the plates, as shown in Figure 2, and assembled in the torsional device *(4)*. This was a load-controlled test and the specimens were loaded at 0.42 N·m/min, so that failure occurred in about 15 min.

Typical test results are shown in Figure 5. The stress-strain relationship for pure grout is nonlinear initially, but with increased loading it becomes linear. Because all specimens failed in tension, the most critical mode of failure for pure grout is obviously tension. The variation of strength, shear strain at failure, and shear modulus with curing time is shown in Figure 6. Because the failure was tensile, the failure stress corresponds to the tensile strength and these results are comparable with results reported from direct tension tests by Vipulanandan and Krizek *(5)*. The strength increased continuously at a reducing rate. The 7-day strength (0.2 MPa) increased by about 40 percent after 1 additional week of curing and a further 25 percent after 28 days of curing. The failure strain decreased rapidly with curing time until the change was negligible after 20 days. The 7-day failure strain (0.85 percent) reduced by 30 percent after 1 additional week and a further 10 percent after 28 days of curing. The shear modulus is defined as the gradient of the stress-strain curve at 50 percent of failure strength. The shear modulus increased rapidly during the initial 2 weeks, with the 7-day modulus doubling during the second week and increasing a further 25 percent after 28 days of curing.

BONDING PROPERTIES

The adhesive tensile strengths obtained from several tests are summarized in Figure 7*a*. The strength increased rapidly during the first 8 days of curing and reached a maximum value of 5.2 kg/cm^2 (0.51 MPa). However, with increased curing the strength reduced to less than 4 kg/cm^2 (0.39 MPa) on the 20th day and to almost 3.5 kg/cm^2 (0.34 MPa) on the 30th day of curing. The variation of adhesive shear strength with curing time is summarized in Figure 7*b*. The adhesive shear strength, τ_f^{AS}, increased rapidly during the first few days, reaching a peak of 3.5 kg/cm^2 (0.34 MPa) around the second week. However, with increased curing, the strength reduced to 2.8 kg/cm^2 (0.27 MPa) after about 3 weeks and 2.5 kg/cm^2 (0.25 MPa) after about 4 weeks. A similar trend in the adhesive

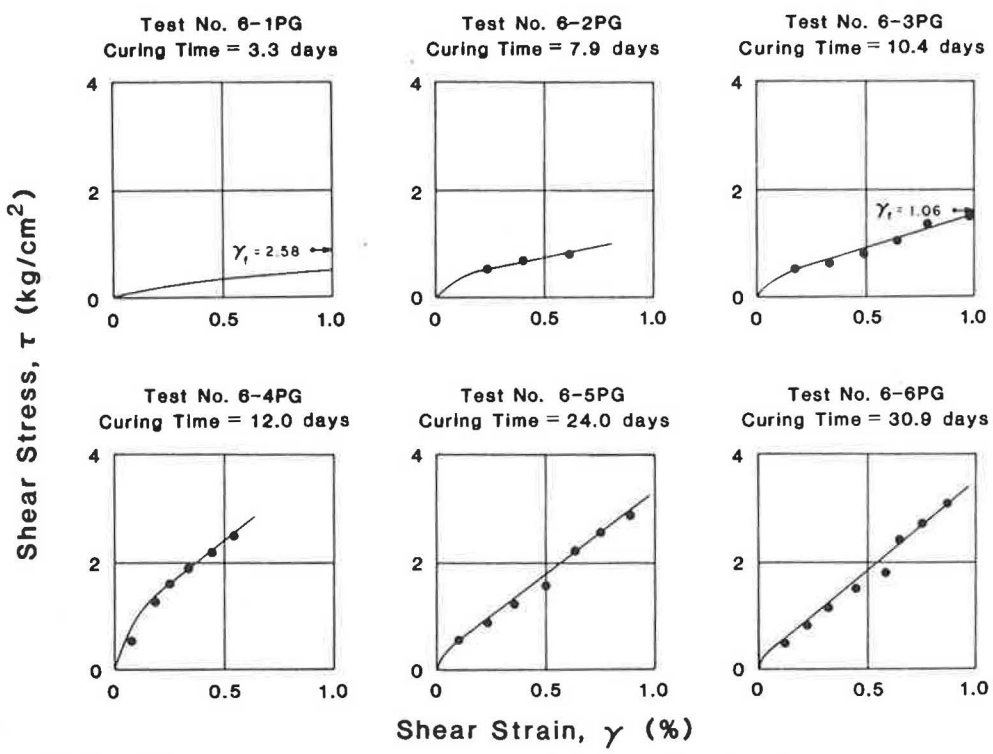

FIGURE 5 Shear stress-strain relationships for pure grout at different curing times.

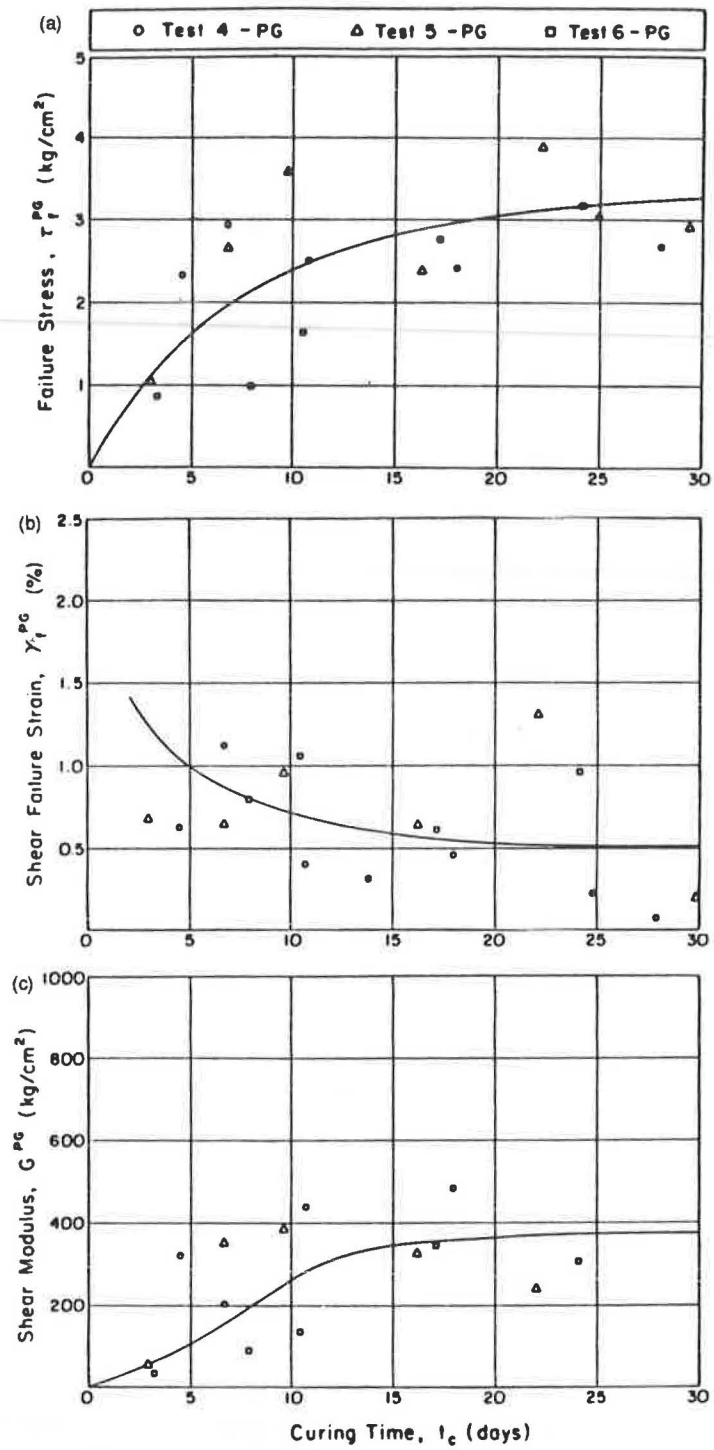

FIGURE 6 Variation of failure stress, shear failure strain, and shear modulus with curing time for pure grout.

tensile strength was observed earlier. The reduction in strength may be caused by *(a)* a continuous chemical reaction at the interface and *(b)* a partial debonding and development of high residual stresses as the grout shrinks and becomes brittle. Although the trend in strength development appears to be generally similar, the adhesive tensile strength is greater than the adhesive shear strength during the period under consideration.

PROPERTIES OF GROUTED SAND

The grouted sand specimens were prepared by injecting grout into sand confined under a K_o condition. As in the case of pure grout, a concentric nylon rod was placed in a plexiglass mold and a known amount of sand was placed and vibrated to obtain a porosity of 0.36 ± 0.02. The test configuration used for these tests was similar to that used for pure grout. Six specimens

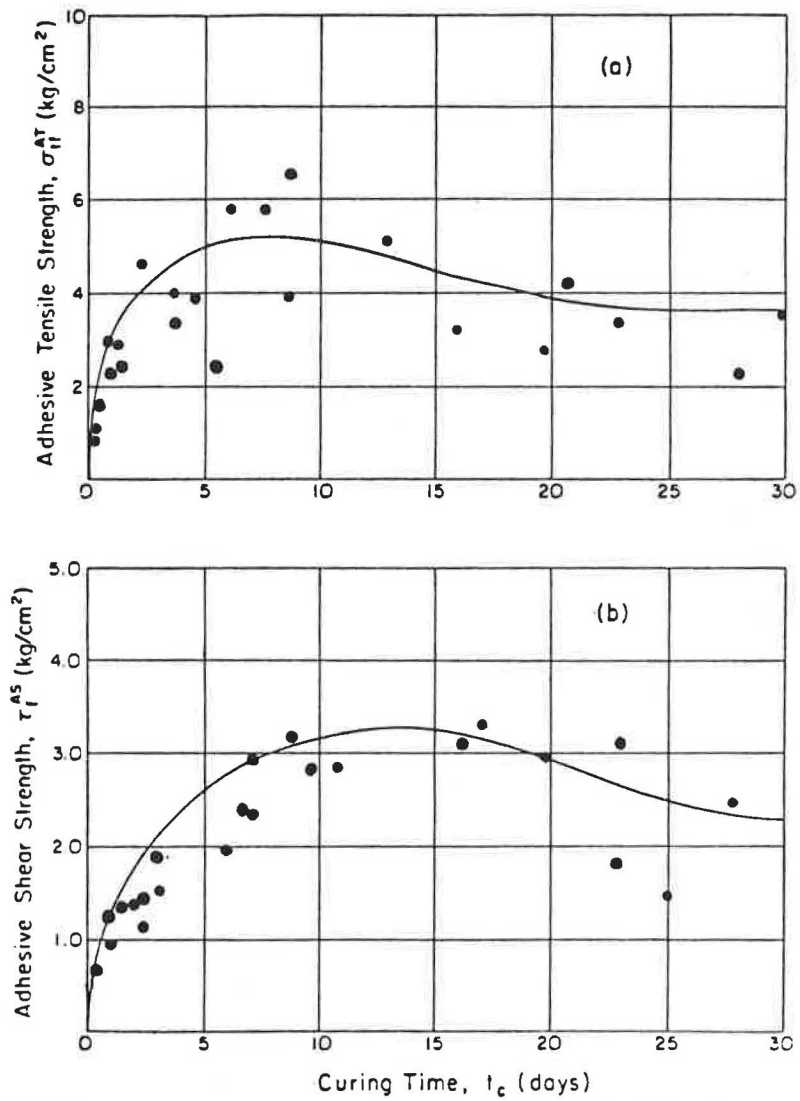

FIGURE 7 Variation of adhesive tensile and shear strengths with curing time.

were grouted in parallel at an injection pressure of approximately 13.8 KPa; about 6 void volumes of grout were passed through each specimen to achieve complete grout saturation *(6)*. Approximately 1 day after grouting, the molds were dismantled and the specimens were removed, sealed in moistened plastic bags, and stored in a humid room at a temperature of 20°C ± 2°C.

For specimens with short curing times, the stress-strain relationship under monotonic torsional loading was nonlinear initially and became linear with increased loading. Longer curing resulted in a linear stress-strain relationship, as shown in Figure 8. All failures were tensile, and hence the most critical mode of failure for grouted sand is also tension. Inspection of the failure surface with a magnifying glass with a magnification factor of 3 indicated both adhesive and cohesive failures.

As shown in Figure 9*a*, the failure stress increased continuously at a decreasing rate during the first 2 weeks and remained unchanged thereafter. The 7-day strength, 3.7 kg/cm^2 (0.36 MPa) increased by 25 percent during the second week of curing. The angular failure strain, as shown in Figure 9*b*, reduces rapidly during the first week and continued to reduce at a decreasing rate, approaching a constant value with longer curing time. The 7-day failure strain (0.43 percent) reduced by 50 percent after 14 days of curing and remained unchanged thereafter. The shear modulus (Figure 9*c*) increased almost linearly up to 14 days of curing and the trend thereafter was uncertain due to scatter in the data. The 7-day modulus, 1200 kg/cm^2 (117 MPa) almost doubled during the second week of curing and increased an additional 30 percent after 28 days.

COMPARISONS

Most of the available mechanical property data in the literature are on the compressive properties of grouts and grouted sands so it is useful to advance some comparisons between shear and compressive properties. Toward this end, solid cylindrical specimens (38 mm in diameter and 85 mm in height) of pure grout and grouted sand were capped with sulfur compound and

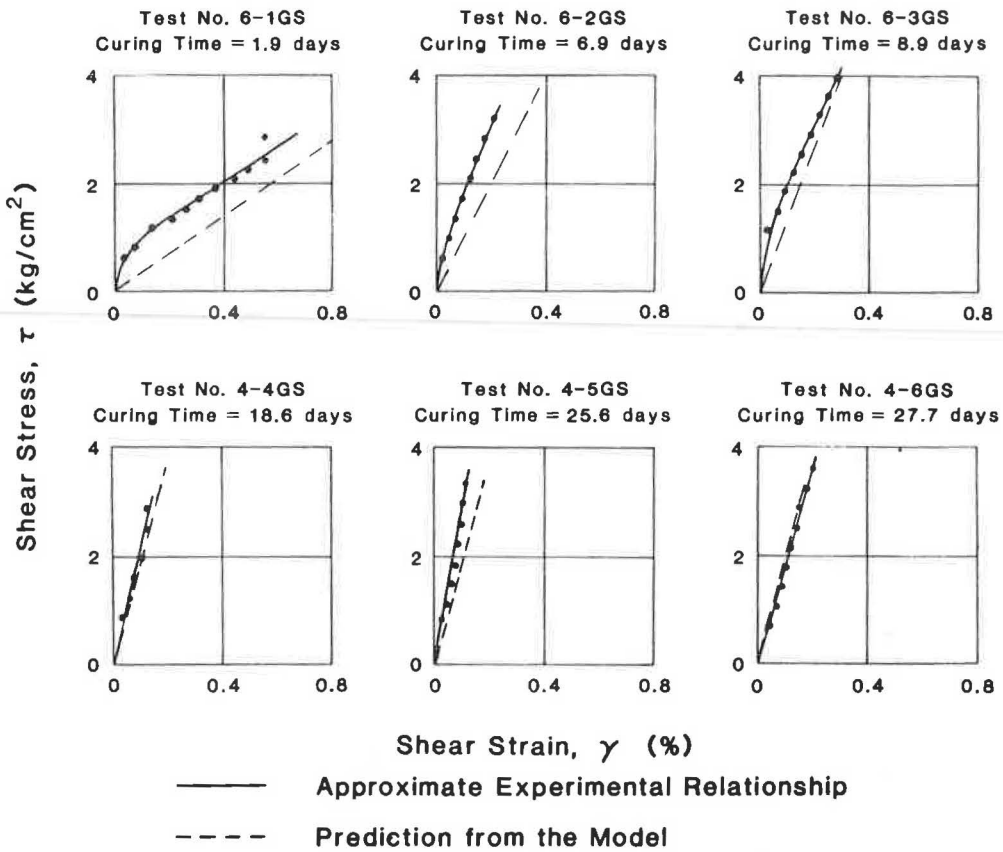

FIGURE 8 Shear stress-strain relationships for grouted sand at different curing times.

tested in unconfined compression at a strain rate of 0.15 percent per minute, and the comparisons in the form of ratios of compressive-to-shear values are given in Table 1.

Grout

The ratio of compressive-to-shear strength increased with curing time and reached a value of 3.2 after 4 weeks. The ratio of failure strains, on the other hand, decreased and approached 2.2 after 4 weeks. The ratio of moduli increased with curing time and reached a value of 3.0 after 4 weeks of curing.

Grouted Sand

The strength ratio decreased with an increase in curing time, from 4.1 after 7 days to 3.3 after 28 days of curing. The ratio of failure strains fluctuated between 1.5 and 2.0 during the period under consideration. The ratio of moduli decreased during the initial 14 days of curing, but remained almost constant thereafter at a ratio of 2.

MODELING BEHAVIOR OF GROUTED SAND

Grouted sand can ideally be considered as consisting of two physically distinct materials. The sand phase consists of discrete particles in contact, while the grout phase fills the voids and holds the particles together. The resulting brittle particulate composite material generally has higher strength and stiffness, both of which change continuously during the process of curing. Available studies on particulate composites have been limited mainly to composites in which the particles are dispersed in the matrix (such as concrete), and hence the interactions between the particles have not been incorporated into the available theories.

During the process of grouting, the grout can be asssumed to fill the voids, although this may often not be the case. As a result of adhesion and shrinkage, self-equilibrating internal stresses, $\bar{P}_G$ and $\bar{P}_S$, are induced within the grouted sand, where $\bar{P}_S$ and $\bar{P}_G$ are defined as the volume-average hydrostatic stresses in the sand skeleton and the grout matrix and may be written as

$$\bar{P}_G = 1/V_G \int_{V_G} P_G(x)\, dV_G \tag{6a}$$

$$\bar{P}_S = 1/V_S \int_{V_S} P_S(x)\, dV_S \tag{6b}$$

where P_S and P_G represent the pointwise hydrostatic stresses in the sand and grout and x designates the position. As there is no external pressure during curing, equilibrium demands that

$$n\bar{P}_G + (1 - n)\,\bar{P}_S = 0 \tag{7}$$

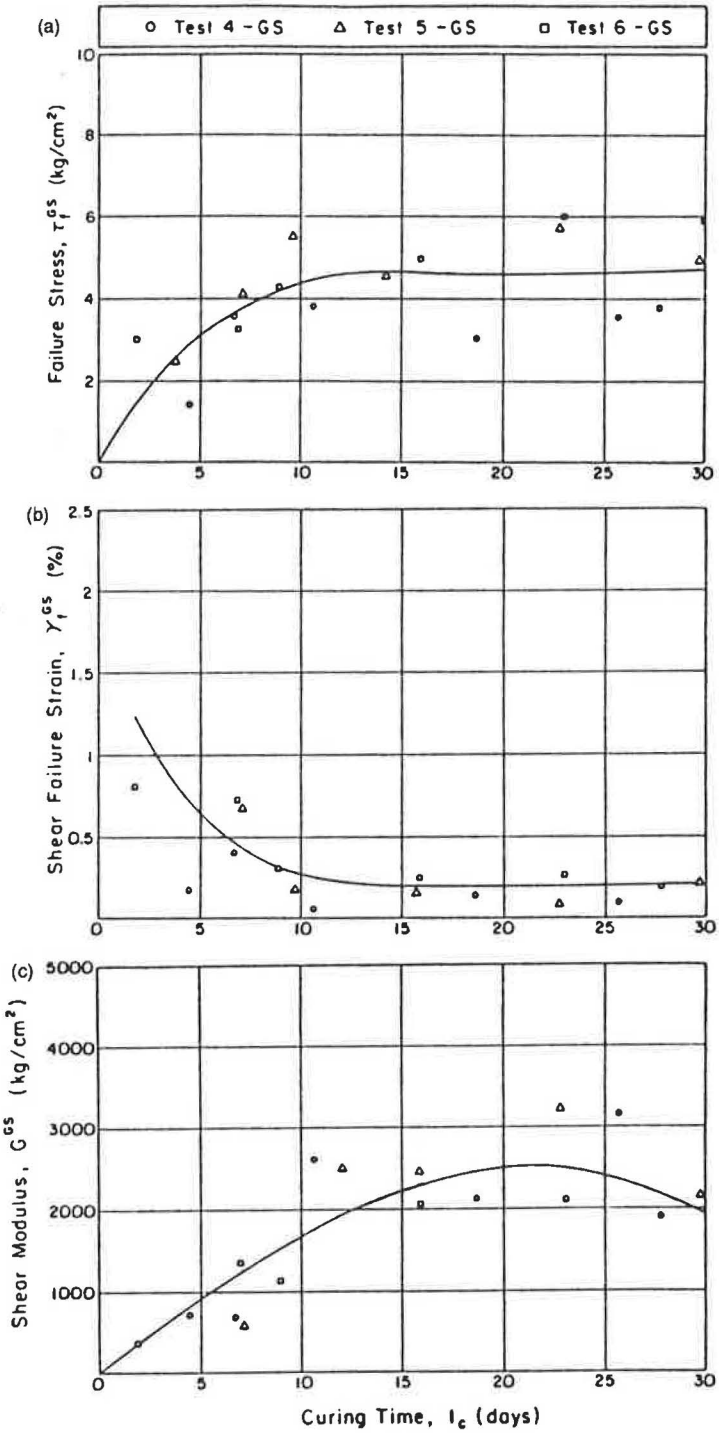

FIGURE 9 Variation of shear properties with curing time for grouted sand.

TABLE 1 RATIOS OF COMPRESSIVE-TO-SHEAR PROPERTIES

Curing Time	Pure Grout (PG)			Grouted Sand (GS)		
	Strength[a]	Failure Strain	Modulus	Strength[a]	Failure Strain	Modulus
7	1.3	–	1.0	4.1	1.7	3.1
14	2.8	3.1	1.7	3.7	2.0	2.1
28	3.2	2.2	3.0	3.3	1.6	1.9

[a]Failure was tensile.

which yields

$$\bar{P}_S = -[n/(1 - n)]\ \bar{P}_G = -e\ \bar{P}_G \quad (8)$$

The induced stresses within the grout matrix will depend on the structure of the soil skeleton, the grout properties, and the method of curing. However, $\bar{P}_G$ cannot exceed the tensile strength of the grout, in which case there would be a failure in the grout matrix during curing. The maximum value of $\bar{P}_S$ will be controlled by the maximum stress transfer that can occur at the interface with no bond failure. In no case will $\bar{P}_S$ exceed the adhesive tensile strength at the sand-grout interface. As a result of $\bar{P}_S$, there is particle-to-particle interaction. Hence, the behavior of grouted sand can be represented as a combination of the behavior of grout and sand without particle interaction (similar to a two-phase dispersed particulate composite) and the behavior of the sand skeleton with particle interaction (the modification that must be made in available theories). The latter is influenced by the initial residual stresses and restraint to particle movement (rolling and sliding) caused by grout acting as a filler material.

Strength Model

Under pure torsional loading the grouted sand failed in tension. At or close to tensile failure the intergranular forces on the failure surface will approach zero. Hence, the effect of particle interaction on such a failure can be neglected. Experimental observations show both adhesive and cohesive failures on the failure surface. Because the failure is tensile, the adhesive tensile strength will play an important role, and it has been shown by Vipulanandan and Krizek *(5)* that the tensile stress on the failure surface can be represented as

$$\sigma_{tf}^{GS}/\sigma_{tf}^{PG} = (1 - n)\ (\sigma_{tf}^{AT}/\sigma_{tf}^{PG}) + n \quad (9)$$

where σ_{tf}^{AT} is the adhesive tensile strength of grout, σ_{tf}^{PG} and σ_{tf}^{GS} are the tensile strengths of pure grout and grouted sand, respectively, and n is the porosity of the sand before grouting. As explained earlier, under pure torsional loading, it is expected that the magnitude of the applied shear stress will be equal to that of the tensile stress in the specimen. Hence, σ_{tf}^{PG} and σ_{tf}^{GS} can be replaced by τ_f^{PG} and τ_f^{GS}, respectively, where τ_f^{PG} and τ_f^{GS} are the shear stresses at failure for pure grout and grouted sand, and Equation 9 can be rewritten as

$$\tau_f^{GS}/\tau_f^{PG} = (1 - n)\ (\sigma_{tf}^{AT}/\tau_f^{PG}) + n \quad (10)$$

Figure 10*a* compares the strength ratios (grouted sand to pure grout) predicted by this model with the experimental data, where values for σ_{tf}^{AT} and τ_f^{PG} were obtained from Figures 7*a* and 6*a*, respectively. Although there is a scatter in the data, the trend in the variation of the strength ratio with curing time is quite adequately represented by the model. Figure 10*b* indicates a satisfactory agreement between the predicted shear strength of grouted sand and the experimental data. Thus, it appears that this model can be used in conjunction with the adhesive and cohesive properties of grout to predict the shear strength of grouted sand.

Stiffness Model

A review of the literature revealed a number of formulas for predicting the modulus of composites based on the modulus and volume concentration of each constituent. However, all of these models have been developed on the basis of very limited or no particle interaction. Because particle interaction plays an important role in the case of grouted sand, any such model must be used cautiously and with appropriate modification.

Hansen *(7)* found that the iso-stress model, also termed the Reuss model, is better than the iso-strain model when the aggregate is stiffer than the matrix, which is the case in grouted sand [the stiffness of quartz sand particles is about 7.5×10^5 kg/cm^2 (7.4×10^4 MPa) *(8)* and that of the grout is on the order of 10^2 kg/cm^2 (9.8 MPa) and changes somewhat with curing time]. Hence, with appropriate modification the iso-stress model can be expressed as

$$1/G^C = (1 - C)/G^m = n/G^m \quad (11)$$

where the modulus of the composite, G^C, can be represented in terms of its matrix modulus, G^m, and volume concentration of particles, C.

As mentioned earlier, the stiffness of grouted sand can be attributed to two factors—particle interaction and the arrangement of rigid particles in a grout matrix. Accordingly, the stiffness of the grouted sand, G^{GS}, can be represented as a linear combination of the two factors, which can be written as

$$G^{GS} = G^S + G^C \quad (12)$$

where G^S is the stiffness due to the particle interaction and G^C is the stiffness of grouted sand without particle interaction. G^S will be influenced by the initial confinement, $\bar{P}_S$, restriction to particle movement, and sand fabric. Because the failure strain of grouted sand is less than 1 percent and particle movement is restricted, G^S can be represented by the initial tangent modulus of sand. When grouted sand is tested in an unconfined condition, the initial confining pressure that will influence G^S is $\bar{P}_S$. As an approximation, we can assume that $\bar{P}_G$ is influenced (controlled) by the uniaxial tensile strength of the grout; hence, a limiting case can be represented as

$$\bar{P}_S = -e\ (\sigma_{tf}^{PG}/3) = -e\ (\tau_{tf}^{PG}/3) \quad (13)$$

Because particle movements (rolling and sliding) are restricted by the grout filler, it is reasonable to approximate the modulus of the sand skeleton, G^S, by the small strain dynamic modulus of sand. According to Richart et al. *(9)*, the dynamic shear modulus, G, for clean rounded sands ($e < 0.80$) can be expressed as

$$G = [700(2.17 - e)^2]/(1 + e)\ (\bar{\sigma}_o)^{0.5} \quad (14)$$

where $\bar{\sigma}_o$ is the mean stress (G and $\bar{\sigma}_o$ are expressed in kg/cm^2). Using $e = 0.56$ and $\bar{\sigma}_o = \bar{P}_S$, it is possible to write the shear modulus as

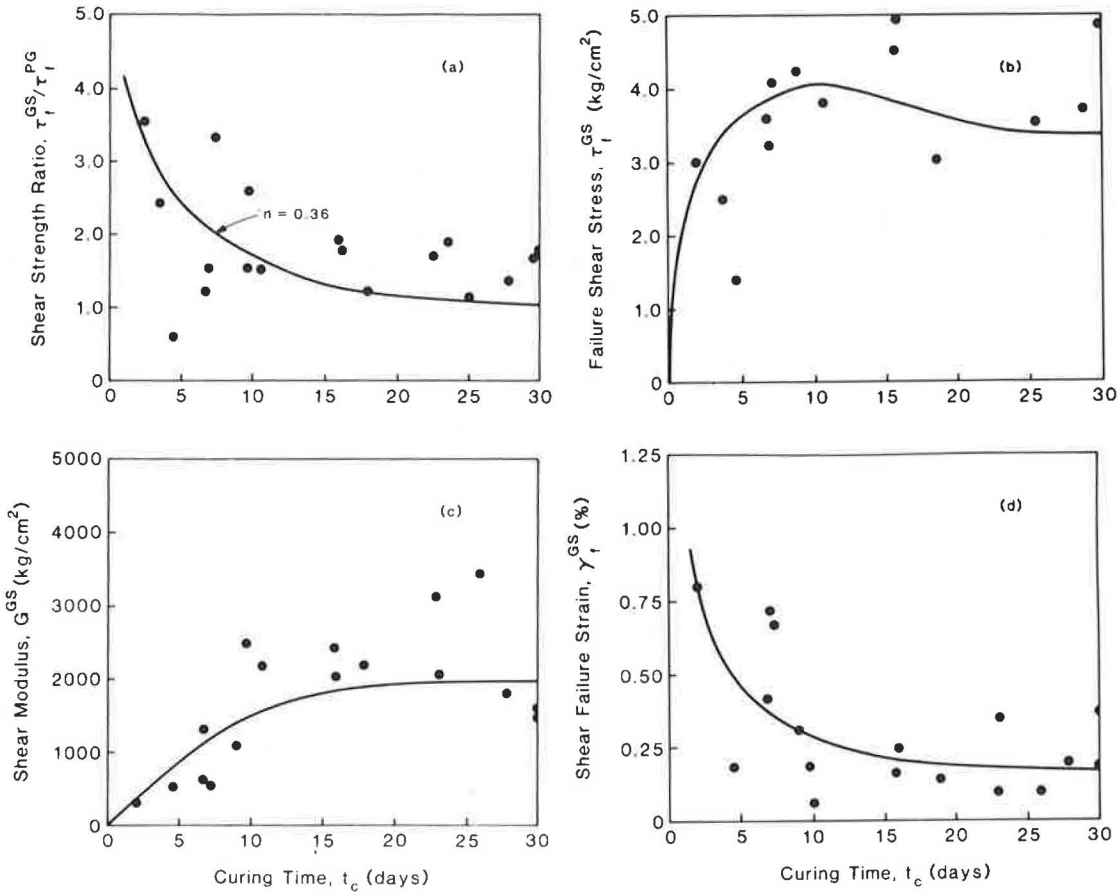

FIGURE 10 Comparison of predicted and measured results for grouted sand.

$$G^S = 500\,(\tau_f^{PG})^{0.5} \tag{15}$$

Therefore, the Reuss model can be modified and the stiffness model for grouted sand can be represented as

$$G^{GS} = G^S + G^{PG}/n \tag{16}$$

Figure 10*c* compares the experimental and predicted shear modulus of grouted sand. The variation in the shear modulus is well represented and the prediction of the magnitude is satisfactory. Hence, this model can be used in conjunction with the properties of grout and sand to predict the stiffness of grouted sand.

Failure Strain Model

It was observed that the stress-strain relationship for grouted sand is approximately linear, and the constitutive relationship can therefore be represented as

$$\tau = G^{GS}\,\gamma \tag{17}$$

where τ is the shear stress and γ is the shear strain. Hence, the failure strain can be written as

$$\begin{aligned}\gamma_f^{GS} &= \tau_f^{GS}/G^{GS} \\ &= (1-n)\,(\sigma_{tf}^{AT} + n\,\tau_f^{PG})/(G^S + G^{PG}/n)\end{aligned} \tag{18}$$

Figure 10*d* compares the experimental results with those predicted by Equation 18. The model represents well the variation of failure strain with curing time, and the prediction of the magnitude is good. Hence, this model can be used in conjunction with the properties of grout and sand to predict the shear strain at failure.

Figure 8 compares the predicted and experimental stress-strain relationships for grouted sand. The predictions were based on the strength model (Equation 9) and stiffness model (Equation 16), which were developed independently based on the proposed theory for grouted sand. Although the agreement was not good for short curing times, the predictions improved with increased curing.

CONCLUSIONS

Based on this complementary experimental and analytical study, the following conclusions can be advanced:

1. The most critical mode of failure for grout and grouted sand under unconfined torsional loading is tension. The strength, failure strain, and modulus of pure grout and grouted

sand change continuously at varying rates during the first month of curing; the strength and modulus were higher for grouted sand than for pure grout, but the inverse was true for the failure strain. Both adhesive and cohesive failures were observed on the failure plane of the grouted sand.

2. The stress-strain relationship of grout and grouted sand under monotonic torsional loading is essentially linear except during the early stages of curing, where it is nonlinear during initial loading but becomes linear with increased loading.

3. The adhesive tensile and shear strengths develop rapidly during initial curing, with the adhesive tensile strength always being greater than the adhesive shear strength. These tests have the potential to be developed as standard testing methods for evaluating the bonding properties of grouts.

4. The behavior of grouted sand can be considered as consisting of two components: one due to interaction of soil particles (such as in ungrouted sand) and the other due to the presence of a grout matrix surrounding the rigid soil particles (as in the behavior of particulate composites). Strength and stiffness models based on this concept give satisfactory results when predictions are compared with the test data. These models offer the potential for predicting the mechanical behavior of grouted sand under torsional loading from a knowledge of the adhesive and cohesive properties of the grout and the porosity of the sand.

REFERENCES

1. A. S. Saada and F. C. Townsend. *State of the Art: Laboratory Strength Testing of Soils*. Special Technical Publication 740. American Society for Testing and Materials, 1981, p. 77.
2. D. W. Hight, A. Gens, and M. J. Symes. The Development of a New Hollow Cylinder Apparatus for Investigating the Effects of Principal Stress Rotation in Soils. *Geotechnique*, 1983, pp. 355–383.
3. R. J. Krizek and C. Vipulanandan. Evaluation of Adhesion in Chemically Grouted Geomaterials. *Geotechnical Testing Journal*. American Society for Testing Materials, Vol. 8, No. 4, 1985, pp. 184–190.
4. C. Vipulanandan. *Interactive Roles of Constituents on the Mechanical Behavior of Chemically Grouted Sand*. Ph.D. dissertation, Department of Civil Engineering, Northwestern University, Evanston, Ill., 1984.
5. C. Vipulanandan and R. J. Krizek. Tensile Properties of Chemically Grouted Sand. In *Transportation Research Record 1008*, TRB, National Research Council, Washington, D.C., 1985, pp. 80–89.
6. D. F. Fawcett. Discussion, *Journal of Soil Mechanics and Foundations Division, ASCE*, Vol. 99, No. SM10, 1973, pp. 638–639.
7. T. C. Hansen. *Creep and Stress Relaxation of Concrete: A Theoretical and Experimental Investigation*. Swedish Cement and Concrete Research Institute, Stockholm, 1960, pp. 37–43.
8. G. J. Cohen and O. Isahi. The Elastic Properties of Three-Phase Composites. *Journal of Composite Materials*, Vol. 1, 1967, pp. 391–403.
9. F. E. Richart, Jr., J. R. Hall, and R. D. Woods. *Vibrations of Soils and Foundations*. Prentice-Hall, Inc., Englewood Cliffs, N.J., 1970.